Fast and Sensitive Solution-Processed Visible-Blind Perovskite UV Photodetectors

*Valerio Adinolfi, Olivier Ouellette, Makhsud I. Saidaminov, Grant Walters, Ahmed L. Abdelhady, Osman M. Bakr, and Edward H. Sargent**

Hybrid perovskites have gained wide attention since their potential in high-efficiency solar cells was demonstrated.[1,2] These semiconductors combine facile and inexpensive fabrication with excellent optoelectronic properties.[3] Recent advances have led perovskite-based solar cells to exceed 22.1% certified power conversion efficiency[4] and visible photodetectors to reach photoconductive gain of 10^4 electrons per photon.[5] The absorption spectrum of perovskite semiconductors can be easily adjusted by tuning the electronic bandgap via fine control over the compound stoichiometry.[6] This technique has been largely used for methylammonium lead halide perovskites and has led to excellent, tunable visible-light absorbing materials.[7–10]

Methylammonium lead chloride ($MAPbCl_3$) is a wide-bandgap semiconductor, transparent to visible but sensitive to UV radiation;[11] such absorption, mainly limited to wavelengths shorter than 400 nm, makes it attractive for visible-blind[12] UV detection applications such as fire and missile plume detection[13] and optical communications,[14] as well as transparent optoelectronics.[15,16] However, to the best of our knowledge, no efficient UV detection devices have yet been developed based on $MAPbCl_3$, a consequence of the poor electronic properties of $MAPbCl_3$ in its traditionally synthesized polycrystalline thin film form.[17]

Recently, $MAPbCl_3$ single crystals of millimeter dimensions have been grown exhibiting excellent optoelectronic properties. A pioneering proof-of-principle UV detector was also produced by leveraging this technology, but the large transverse dimensions of the device—several times larger than the carrier diffusion length—severely impeded its performance.[18] Most photoexcited carriers would therefore recombine before being extracted and would thus not contribute to the detection signal. Our much smaller device length (5 μm compared to the previous 350 μm) allows us to extract successfully a higher number of photoexcited carriers, and thus obtain a significantly better performance.

We hypothesized that $MAPbCl_3$ single crystals could overcome the limits exhibited by thin films and that a substrate-integrated approach could enable efficient devices through better control of the absorbing layer thickness. The crystals were synthesized directly on a glass substrate with prepatterned indium tin oxide (ITO) electrodes by inverse temperature crystallization (ITC) and related methods,[19–22] which exploits the drop in solubility of perovskite solutions at high temperature. To grow crystalline films rather than freestanding single crystals, we modified the previously used approach by stirring the solution during crystallization[5] in order to increase the nucleation rate within the solution, thus producing multiple interconnected crystals. To obtain homogeneous crystalline films, we used diluted solutions (0.25 M instead of 1 M in ITC). Saturation was then reached by adding toluene, an antisolvent, into solution. Due to its low boiling temperature, toluene can then be removed easily by heating the film at 145 °C, thus leaving a highly crystalline material behind. As shown in **Figure 1**a, scanning electron microscopy (SEM) reveals that the glass substrate is covered with a dense layer of interconnected $MAPbCl_3$ single crystals with dimensions of ≈15 μm. Additional SEM images are included in the Supporting Information. The rectangular shape of the crystals, which is expected considering the cubic crystallographic structure of this material at room temperature, is evident in Figure 1a.

To investigate the quality of the crystals, we proceeded with the characterization of absorption and photoluminescence (PL), shown in Figure 1b. We observed a steep absorption edge located at ≈430 nm and a PL peak centered close by at 420 nm, indicating good crystal quality. A shoulder is apparent on the PL spectrum, consistent with previous reports,[23–25] and is attributed to Urbach tail states.[26] The crystalline film, as expected, is completely transparent at visible wavelengths and absorbs light at UV frequencies. We then performed X-ray diffraction (XRD) to identify the crystallographic structure of the crystal. The analysis returns the Bragg reflection peaks of a perovskite cubic structure as expected for $MAPbCl_3$.

Encouraged by these initial results, we sought to investigate the electrical properties of the crystals and compare their performance to that of thin films. Photoluminescence decay has been widely used as a figure of merit for carrier recombination within semiconductors.[24] We therefore performed this measurement on single crystals and thin films as shown in **Figure 2**a,b, respectively. The thin films were fabricated via spin-coating of

Dr. V. Adinolfi, O. Ouellette, G. Walters,
Prof. E. H. Sargent
Department of Electrical and Computer Engineering
University of Toronto
10 King's College Road, Toronto, Ontario M5S 3G4
Canada
E-mail: ted.sargent@utoronto.ca

Dr. M. I. Saidaminov, Dr. A. L. Abdelhady,[+]
Prof. O. M. Bakr
Division of Physical Sciences and Engineering
Solar and Photovoltaics Engineering Center
King Abdullah University of Science
and Technology (KAUST)
Thuwal 23955-6900, Saudi Arabia

[+]Present address: Department of Nanochemistry, Istituto Italiano di Tecnologia, Via Morego 30, 16163 Genova, Italy

DOI: 10.1002/adma.201601196

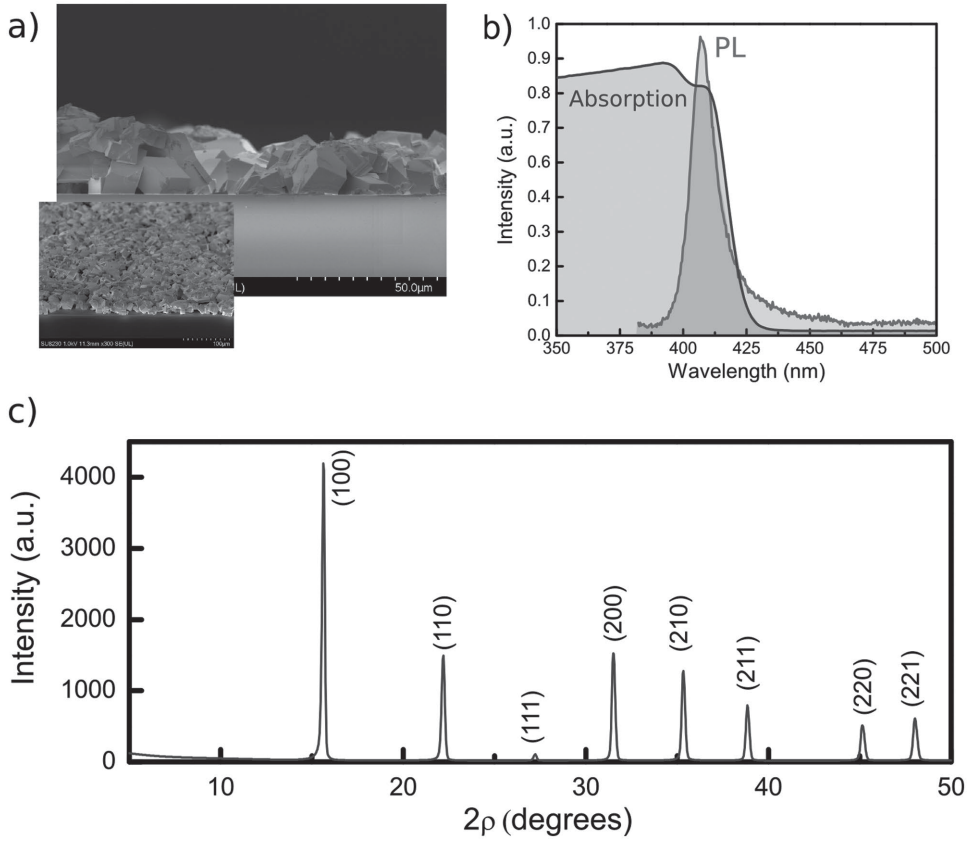

Figure 1. Assessment of the structural and material quality of the synthesized perovskites single-crystals. a) Cross-section and top-view (inset) SEM image of a $MAPbCl_3$ crystalline film. b) Absorption and photoluminescence spectra. c) XRD data.

a solution of precursors, as reported previously,[11] and their average grain size is 55 nm, two orders of magnitude smaller than the crystalline films reported herein. A biexponential fit of the PL decay curves reveals a slow component of 31 ns and a fast component of 4 ns in the crystal, ascribed to bulk and surface photocarriers lifetime, respectively.[24] A much faster decay of 6 ns in the thin film, dominated by the fast component, suggests severe recombination of photocarriers at grain boundaries.

We further explored the properties of $MAPbCl_3$ single crystals by measuring their charge carrier mobility. Hall effect measurement returned a high hole mobility of 26 $cm^2\ V^{-1}\ s^{-1}$. This measurement also revealed a low concentration of majority carriers (holes) of $10^{10}\ cm^{-3}$, indicating that the semiconductor is intrinsic. The data for the Hall effect measurement is included in the Supporting Information.

The observed good mobility and low concentration of free carriers are important properties for a material to produce efficient light detectors.[27,28] These quantities directly impact the responsivity, speed, and dark current of the detectors. We therefore proceeded to fabricate substrate-integrated $MAPbCl_3$

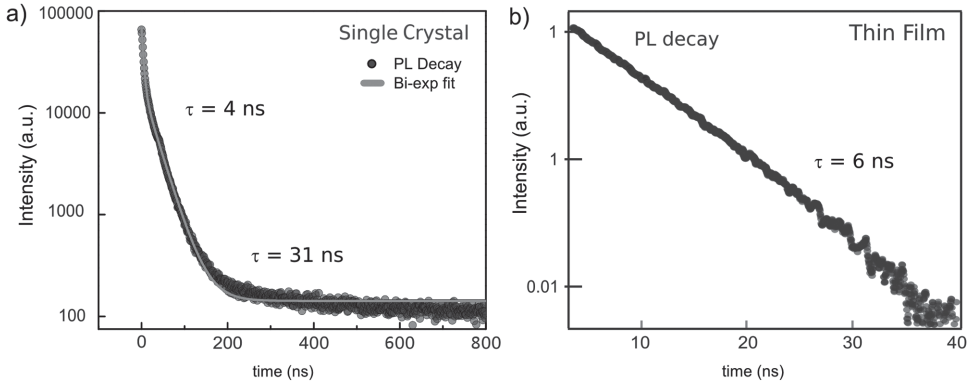

Figure 2. Comparison of single-crystal and thin film perovskite dynamics. a) PL decay trace of $MAPbCl_3$ single crystals and biexponential fitting. b) PL decay trace of a $MAPbCl_3$ thin film.

Adv. Mater. **2016**,
DOI: 10.1002/adma.201601196

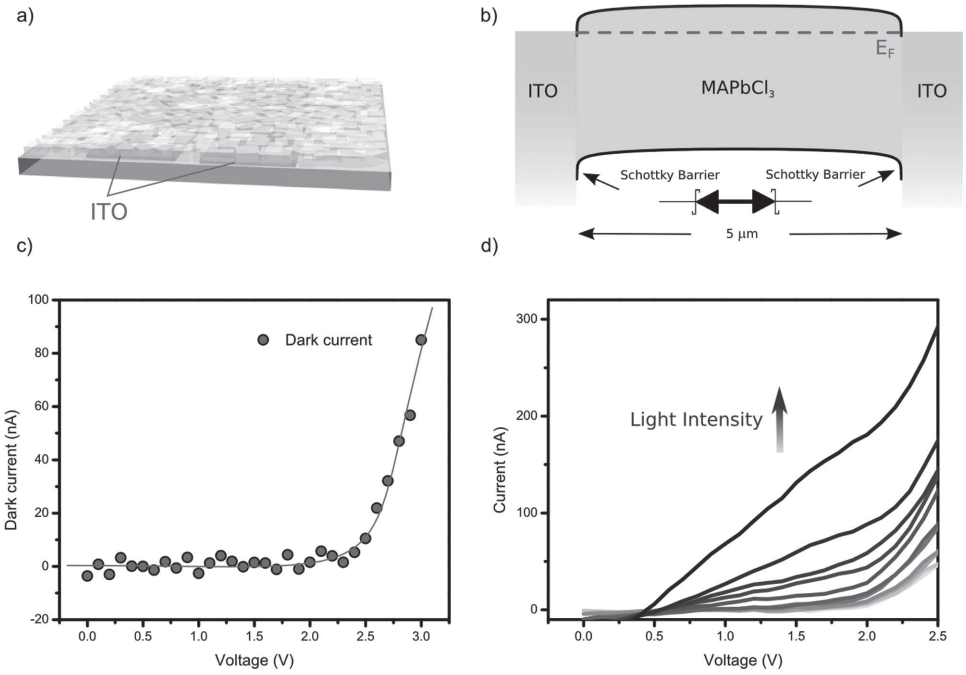

Figure 3. Photodetector structure and operation. a) 3D model of the $MAPbCl_3$ UV detectors. b) Spatial band diagram of the device. c) Dark and d) light current–voltage characteristic of the UV detector.

UV detectors and evaluated their performance. As shown in **Figure 3**a,b, we used glass substrates with prepatterned ITO contacts that were defined using standard photolithography and hydrochloric acid etching. The spacing between the ITO electrodes, defining the detector's active area which is equivalent to the length of the least-resistance path between the contacts, is 5 µm. The active area is thus mainly covered by single domains, and the relatively few grain boundaries that will be involved along the transport path will have limited impact on performance in light of their rarity. We measured the current–voltage characteristic of the detector in the dark (Figure 3c) and under 385 nm monochromatic illumination (Figure 3d). As shown in Figure 3c the ITO/$MAPbCl_3$ junction produces rectification, thus enabling low dark current. The current benefits from a strong contribution of photogenerated carriers under illumination, as shown in Figure 3d, where photocurrent is reported at several light intensities. It can also be noted that the combination of a glass substrate and ITO electrodes allows for a fully transparent device (the absorption spectrum of the full detector is shown in Figure S3 of the Supporting Information).

We further characterized the device by carrying out a quantitative analysis of detector performance. First, we measured the responsivity as a function of the light intensity (λ = 385 nm) as shown in **Figure 4**a. The responsivity decreases at high incident light intensities following the characteristic behavior of photoconductive gain.[29–31] This mechanism has been attributed in previous reports to electronic trap states at the perovskite-ITO interface. These enable the transition of the contact from rectifying in the dark to ohmic under illumination,[9] as is apparent in Figure 3c,d. Under these conditions, gain will be obtained when the recombination lifetime of the photocarriers exceeds their transit time through the device.[5] This condition is satisfied in the present study by virtue of the long carrier lifetime and the high charge carrier mobility in the crystals. In fact, at low power (≈4 nW) we measured a responsivity of ≈18 A W^{-1} corresponding to an external gain (defined as electrons/incident photons) approaching 100. This result represents a 2000-fold improvement compared to previously reported $MAPbCl_3$ detectors.[18] Combining the information on the dark current and the responsivity, we can calculate the detectivity[32] defined as $D^* = \frac{R\sqrt{A}}{\sqrt{q\,I_{dark}}}$, yielding ≈$10^{12}$ Jones. This result also represents a 2-order of magnitude improvement over previously reported UV detectors.[18]

We further investigated the dynamic performance of the UV detector by measuring its response time. In the present case, response time is mainly determined by the lifetime of the electronic trap states at the semiconductor–metal interface. In fact, if these traps stay filled for a long time after illumination, speed will be limited by a slower fall time, as is observed in Figure 4b. Fall time is measured to be 1 ms, which improves by a factor of 50 on previous reports on $MAPbCl_3$ detectors. We finally measured the spectral photocurrent and, as expected, found that the response follows well the behavior of the absorbance of $MAPbCl_3$, presenting a steep rising edge positioned at ≈420 nm. The device is therefore completely transparent to visible radiation and sensitive exclusively to UV light. Figure 4c also shows a desirably flat response for above-bandgap radiation.

To compare performance, thin-film photodetectors were also fabricated in the same architecture, using the aforementioned method.[11] These thin-film photodetectors exhibit responsivities below 10^{-3} A W^{-1} and a fall time of 20 ms (Figure S4, Supporting Information). These findings confirmed the advantageous performance of the single-crystalline materials and devices presented herein.

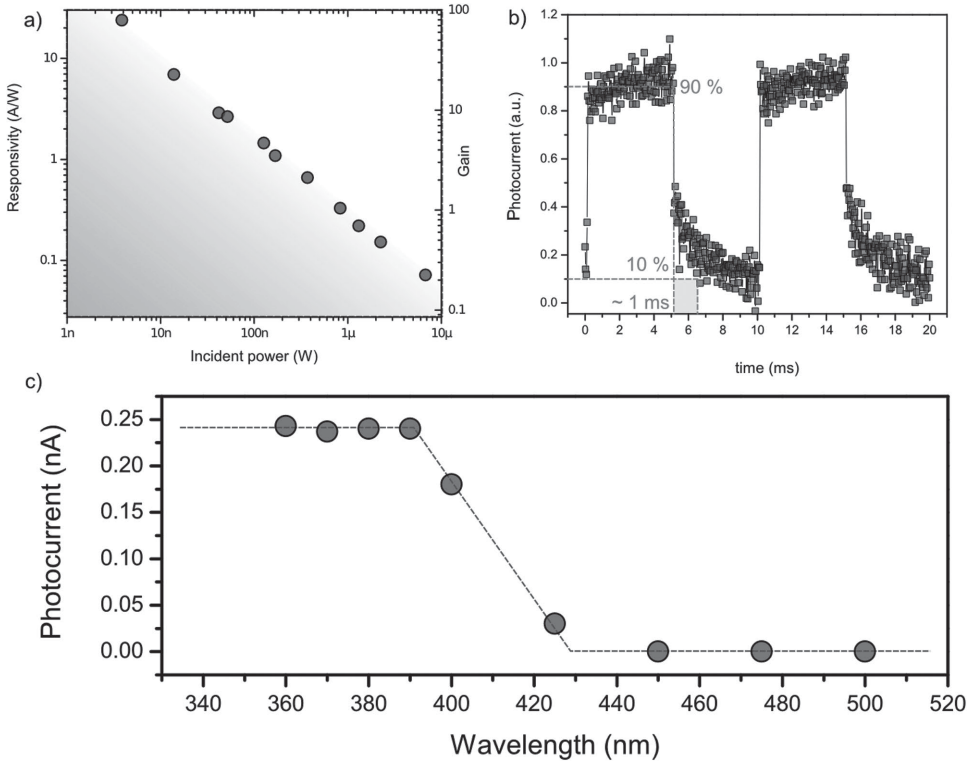

Figure 4. Performance of the photodetectors. a) Responsivity and gain as a function of incident light power. The detector was biased at 5 V. b) Response time of the $MAPbCl_3$ UV detector. c) Spectral photocurrent.

Other materials have also been investigated for visible-blind UV detection, such as zinc oxide (ZnO)[33,34] and tin oxide (SnO_2).[35,36] However, solution-processed, visible-blind photodetectors based on these materials exhibit either very slow time responses of well over one second[35–38] or low responsivities (under 0.1 A W^{-1}).[39,40] The photodetector presented herein is the first solution-processed, relatively fast, and responsive visible-blind photodetector.

In conclusion, in this work we present the first visible-blind UV photodetector based on $MAPbCl_3$ integrated on a substrate. The detector exhibits excellent performance, improving all the relevant figures of merit by several orders of magnitude compared to previous reports. The potential of wide bandgap perovskite semiconductors, potentially including other variants such as $CsPbCl_3$, makes them promising candidates for light detection and transparent electronics. Achieving such good performance was possible only by using substrate-integrated single crystals overcoming the severe limitations affecting thin films due to poor electronic properties. This work opens the way to future developments; in particular the dark current and the noise current as a consequence, could be decreased by improving the contact/semiconductor interface. The high bandgap of the semiconductor could, in fact, enable lower dark current and higher detectivity.

Experimental Section

$MAPbCl_3$ Crystallization: 10 mL of a 0.25 M solution of $PbCl_2$/MACl (1/1 in dimethyl sulfoxide (DMSO)/dimethylformamide (DMF) 1/1 v) was mixed with 5 mL of toluene and poured into an 80 mm crystallizing dish containing the substrates and a stirring bar. The crystallizing dish was covered with aluminum foil and placed onto a hot plate. The temperature of the hotplate was brought up to 95 °C. The stirring bar was activated at a speed of 400 rpm. These conditions were maintained for 40 min, the time necessary to grow a compact film of interconnected $MAPbCl_3$ crystals. Right after crystallization the substrates were annealed for 5 min at a temperature of 145 °C to promote adhesion of the crystals with the glass substrate.

Absorption Measurements: Absorption measurements were performed using a Perkin Elmer lambda 950 spectrometer.

XRD: The data were collected from $MAPbCl_3$ single crystal powder using a Siemens D5000 Bragg-Brentano diffractometer.

Photoluminescence: The excitation source used to obtain photoluminescence spectrum was a light conversion Pharos laser with an Orpheus OPA emitting 200 fs pulses at a wavelength of 360 nm and with a repetition rate of 5 kHz. Photoluminescence was collected with a multimode fiber and measured using an Ocean Optics USB 2000 spectrometer.

Photoluminescence Decay: Time dependent PL traces were acquired using a Horiba Fluorolog time correlated single photon counting system.

Current–Voltage Characterization: IV measurements were performed using a Keithley 2400 SourceMeter. The detector was contacted using microprobes. The sample was kept in a closed, dark, shielded environment in a controlled N_2 atmosphere. Measurements performed in air are shown in the Supporting Information. For the light characterization a 385 nm monochromatic illumination was provided using a light-emitting diode (LED) put in direct contact with the sample. The illumination intensity was controlled using a circular aperture.

UV Detector Fabrication: Glass substrates with predeposited ITO were patterned using standard photolithography and HCl (hydrochloric acid) etching. Interdigitated contacts were obtained with a channel length of 5 μm and a channel width of 1 mm. A layer of interconnected $MAPbCl_3$ single crystals, with dimensions of ≈15 μm, was then deposited on the substrate using the method previously described.

Adv. Mater. **2016**,
DOI: 10.1002/adma.201601196

Responsivity Measurements: Responsivity (R) was calculated by measuring the photocurrent I_{ph} (obtained by subtracting the dark IV from the light IV) and dividing this value by the incident power P_{inc}, such that $R = I_{ph}/P_{inc}$. To measure P_{inc} the following procedure was used: The illumination (λ = 385 nm, LED light) was controlled using a circular aperture with an area, A. The optical power coming through the aperture (P_{opt}) was measured using a Newport 1830c power meter. The incident power was then calculated using the relation $P_{inc} = A_{det} \times P_{opt}/A$, where A_{det} is the active area of the detector (0.005×1 mm).

Time Response Characterization: Monochromatic (λ = 385 nm) illumination, with a power of 2 μW, was provided by using an LED. The light source was time-modulated using a function generator. The response of the photodetector was amplified using a Stanford Research Systems SR570 current preamplifier and measured using an Agilent Infiniium DSO 84 digital oscilloscope. During the measurement the device was biased using a Keithley 2400 SourceMeter. The sample was kept in a sealed, dark environment, in a controlled N_2 atmosphere.

Spectral Photocurrent Measurement: The spectral photocurrent was measured using a Stanford Research SR 830 lock-in amplifier. The monochromatic illumination was provided by a monochromator supplied with a xenon lamp (solar simulator). The light intensity was kept constant (P_{inc} = 100 pW) over the wavelength sweep by using a neutral density filter. The light excitation was chopped at a frequency of 15 Hz. The device was biased using a Keithley 2400 SourceMeter. The detector was kept in a dark, shielded environment.

Supporting Information

Supporting Information is available from the Wiley Online Library or from the author.

Acknowledgements

V.A. and O.O. contributed equally to this work.

Received: March 1, 2016
Revised: April 30, 2016
Published online:

[1] H.-S. Kim, C.-R. Lee, J.-H. Im, K.-B. Lee, T. Moehl, A. Marchioro, S.-J. Moon, R. Humphry-Baker, J.-H. Yum, J. E. Moser, M. Grätzel, N.-G. Park, *Sci. Rep.* **2012**, *2*, 591.
[2] A. Kojima, K. Teshima, Y. Shirai, T. Miyasaka, *J. Am. Chem. Soc.* **2009**, *131*, 6050.
[3] S. D. Stranks, G. E. Eperon, G. Grancini, C. Menelaou, M. J. P. Alcocer, T. Leijtens, L. M. Herz, A. Petrozza, H. J. Snaith, *Science* **2013**, *342*, 341.
[4] *National Renewable Energy Laboratory (NREL)*, Best Research-Cell Efficiencies Chart (as of March 2016), **2016**.
[5] M. I. Saidaminov, V. Adinolfi, R. Comin, A. L. Abdelhady, W. Peng, I. Dursun, M. Yuan, S. Hoogland, E. H. Sargent, O. M. Bakr, *Nat. Commun.* **2015**, *6*, 8724.
[6] G. Xing, N. Mathews, S. S. Lim, N. Yantara, X. Liu, D. Sabba, M. Grätzel, S. Mhaisalkar, T. C. Sum, *Nat. Mater.* **2014**, *13*, 476.
[7] H.-R. Xia, J. Li, W.-T. Sun, L.-M. Peng, *Chem. Commun.* **2014**, *50*, 13695.
[8] Y. Fang, J. Huang, *Adv. Mater.* **2015**, *27*, 17, 2804–2810, DOI 10.1002/adma.201500099.
[9] R. Dong, Y. Fang, J. Chae, J. Dai, Z. Xiao, Q. Dong, Y. Yuan, A. Centrone, X. C. Zeng, J. Huang, *Adv. Mater.* **2015**, *27*, 1912.
[10] L. Dou, Y. M. Yang, J. You, Z. Hong, W.-H. Chang, G. Li, Y. Yang, *Nat. Commun.* **2014**, *5*, 5404.
[11] R. Comin, G. Walters, E. S. Thibau, O. Voznyy, Z.-H. Lu, E. H. Sargent, *J. Mater. Chem. C* **2015**, *3*, 8839.
[12] L. Sang, M. Liao, M. Sumiya, *Sensors* **2013**, *13*, 10482.
[13] F. Neele, R. Schleijpen, in *Proc. SPIE 5075, Targets Backgrounds IX Charact. Represent.*, SPIEOrlando, FL, USA **2003**.
[14] Z. Xu, B. M. Sadler, *IEEE Commun. Mag.* **2008**, *46*, 67.
[15] J. F. Wager, *Science* **2003**, *300*, 1245.
[16] K. Nomura, H. Ohta, K. Ueda, T. Kamiya, M. Hirano, H. Hosono, *Science* **2003**, *300*, 1269.
[17] S. T. Williams, F. Zuo, C.-C. Chueh, C.-Y. Liao, P.-W. Liang, A. K.-Y. Jen, *ACS Nano* **2014**, *8*, 10640.
[18] G. Maculan, A. D. Sheikh, A. L. Abdelhady, M. I. Saidaminov, M. A. Haque, B. Murali, E. Alarousu, O. F. Mohammed, T. Wu, O. M. Bakr, *J. Phys. Chem. Lett.* **2015**, *6*, 3781.
[19] Y. Liu, Z. Yang, D. Cui, X. Ren, J. Sun, X. Liu, J. Zhang, Q. Wei, H. Fan, F. Yu, X. Zhang, C. Zhao, S. Liu, *Adv. Mater.* **2015**, *27*, 5176.
[20] T. Zhang, M. Yang, E. E. Benson, Z. Li, J. van de Lagemaat, J.M. Luther, Y. Yan, K. Zhu, Y. Zhao, *Chem. Commun.* **2015**, *51*, 7820.
[21] J. M. Kadro, K. Nonomura, D. Gachet, M. Gratzel, A. Hagfeldt, *Sci. Rep.* **2015**, *5*, 11654.
[22] M. I. Saidaminov, A. L. Abdelhady, B. Murali, E. Alarousu, V. M. Burlakov, W. Peng, I. Dursun, L. Wang, Y. He, G. Maculan, A. Goriely, T. Wu, O. F. Mohammed, O. M. Bakr, *Nat. Commun.* **2015**, *6*, 7586.
[23] Y. Fang, Q. Dong, Y. Shao, Y. Yuan, J. Huang, *Nat. Photonics* **2015**, *9*, 679.
[24] D. Shi, V. Adinolfi, R. Comin, M. Yuan, E. Alarousu, A. Buin, Y. Chen, S. Hoogland, A. Rothenberger, K. Katsiev, Y. Losovyj, X. Zhang, P. A. Dowben, O. F. Mohammed, E. H. Sargent, O. M. Bakr, *Science* **2015**, *347*, 519.
[25] A. A. Zhumekenov, M. I. Saidaminov, A. Haque, E. Alarousu, S. P. Sarmah, B. Murali, I. Dursun, X. Miao, A. L. Abdelhady, T. Wu, O. F. Mohammed, O. M. Bakr, *ACS Energy Lett.* **2016**, *1*, 32.
[26] S. John, C. Soukoulis, M. H. Cohen, E. Economou, *Phys. Rev. Lett.* **1986**, *57*, 1777.
[27] C. H. Chen, S. J. Chang, Y. K. Su, G. C. Chi, J. Y. Chi, C. A. Chang, J. K. Sheu, J. F. Chen, *IEEE Photonics Technol. Lett.* **2001**, *13*, 848.
[28] R. Soref, L. Fellow, I. Paper, *IEEE J. Sel. Top. Quantum Electron.* **2006**, *12*, 1678.
[29] E. Muñoz, E. Monroy, J. A. Garrido, I. Izpura, F. J. Sánchez, M. A. Sánchez-Garcı a, E. Calleja, B. Beaumont, P. Gibart, *Appl. Phys. Lett.* **1997**, *71*, 870.
[30] E. Lhuillier, S. Keuleyan, P. Zolotavin, P. Guyot-Sionnest, *Adv. Mater.* **2013**, *25*, 137.
[31] G. Konstantatos, I. Howard, A. Fischer, S. Hoogland, J. Clifford, E. Klem, L. Levina, E. H. Sargent, *Nature* **2006**, *442*, 180.
[32] R. C. Jones, *J. Opt. Soc. Am.* **1960**, *50*, 1058.
[33] F. Omnès, E. Monroy, E. Muñoz, J.-L. Reverchon, *SPIE* **2007**, *6473*, 64730E.
[34] K. Liu, M. Sakurai, M. Aono, *Sensors* **2010**, *10*, 8604.
[35] L. Hu, J. Yan, M. Liao, L. Wu, X. Fang, *Small* **2011**, *7*, 1012.
[36] H. Chen, L. Hu, X. Fang, L. Wu, *Adv. Funct. Mater.* **2012**, *22*, 1229.
[37] W. Tian, T. Zhai, C. Zhang, S. L. Li, X. Wang, F. Liu, D. Liu, X. Cai, K. Tsukagoshi, D. Golberg, Y. Bando, *Adv. Mater.* **2013**, *25*, 4625.
[38] S. I. Inamdar, K. Y. Rajpure, *J. Alloys Compd.* **2014**, *595*, 55.
[39] J. H. Jun, H. Seong, K. Cho, B. M. Moon, S. Kim, *Ceram. Int.* **2009**, *35*, 2797.
[40] B. Gupta, A. Jain, R. M. Mehra, *J. Mater. Sci. Technol.* **2010**, *26*, 223.